Assessment of different methods for characterization and simulation of post-cracking behavior of self-compacting steel fiber reinforced concrete

Fatemeh Soltanzadeh[1], Vitor M.C.F. Cunha, Joaquim A.O. Barros

ISISE, Institute of Science and Innovation for Bio-Sustainability (IB-S), Department of Civil Engineering, University of Minho, Guimarães, Portugal

Abstract

The post-cracking tensile properties of steel fiber reinforced concrete (SFRC) is one of the most important aspects that should be considered in design of SFRC structural members. The parameters that describe the post-cracking behavior of SFRC in tension are often derived using indirect methods combined with inverse analysis techniques applied to the results obtained from three- or four-point prism bending tests or from determinate round panel tests. However, there is still some uncertainty regarding the most reliable methodology for evaluating the post-cracking behavior of SFRC. In the present study a steel fiber reinforced self-compacting concrete (SFRSCC) was developed and its post-cracking behavior was investigated through an extensive experimental program composed of small determinate round panel and prism bending tests. Based on the results obtained from this experimental program, the constitutive tensile laws of the developed SFRSCC were obtained indirectly using two numerical approaches, as well as three available analytical approaches based on standards for estimating the stress versus crack width relationship ($\sigma - w$). The predictive performance of both the numerical and analytical approaches employed for estimating the $\sigma - w$ relationship of the SFRSCC was assessed. The numerical simulations have provided a good prediction of the post-cracking behavior of the concrete. All the analytical formulations also demonstrated an acceptable accuracy for design purposes. Anyhow, among all the employed approaches, the one that considers the results of small determinate round panel tests (rather than that of prism bending tests) has predicted more accurately the constitutive tensile laws of the SFRSCC.

Keywords:

Fiber reinforced self-compacting concrete; Post-cracking behavior; Small determinate round panel; Inverse analysis.

[1] Corresponding author.
E-mail address: soltanzadehfaranak@gmail.com (Fatemeh Soltanzadeh).

1. Introduction

During the past decades, steel fiber reinforced concrete (SFRC) has gained popularity within the construction industry, due to the advantages provided by the fiber reinforcement. Application of steel fibers in concrete technology as a reinforcement system improves the behavior of cement-based materials, mainly in post-cracking stage (Cuenca and Serna 2013). The fibers offer resistance to the formation and propagation of cracks in the concrete matrix and, consequently, improve significantly the post-cracking residual strength and fracture energy of cement-based materials, due to the additional energy required for debonding and pulling out the fibers bridging an active crack (Cunha 2010).

The post-cracking tensile strength of fiber reinforced concrete is one of the most important properties that should be considered when designing structural members made by this composite. Evaluating the residual tensile strengths of SFRC after cracking enables the assessment of the material constitutive relationships for design (CEB-FIP Model Code 2010). If a reliable material constitutive relationship is defined for SFRC, the structural elements can be designed with confidence (Amin *et al*. 2017). Other alternatives are the consideration of the fiber pullout constitutive law, fiber orientation profile and fiber distribution, as demonstrated in Barros and Foster (2018) and in Valente (2019) for the, respectively, shear and flexural reinforcement of SFRC structural elements. However, the exigencies for design application of these approaches are higher, thereby a cohesive tensile stress versus crack width relationship ($\sigma - w$) or a stress versus strain relationship ($\sigma - \varepsilon$) are often used for simulating the fiber reinforcement mechanisms. When modelling the behavior of a concrete with low content of steel fibers (i.e. 0.3% < fiber volume fraction (V_f) < 1.0%), where multiple cracking does not occur (currently designated by tensile strain softening FRC), the $\sigma - w$ relationship is the most appropriate approach to define the post-cracking response of these composites (Abrishambaf *et al*. 2015).

It is widely acknowledged that the uniaxial tensile test is the most accurate method for evaluating directly the post-cracking $\sigma - w$ relationship of SFRC (Amin *et al*. 2017, Stähli 2008). However, direct tensile tests can be quite time-consuming, since they require specialized testing equipment, as well as a careful preparation of the test set-up and specimens (Amin *et al*. 2015, Stähli 2008). Therefore, extensive efforts have been made to assess indirectly the $\sigma - w$ response of SFRC by means of inverse analysis procedures that consider the experimental results obtained by simpler test configurations. Distinct test typologies may be employed to indirectly assess the $\sigma - w$ response, such as: either three- or four-point bending tests on prismatic specimens (Barros *et al*. 2005, di Prisco 2013, Soltanzadeh *et al*. 2014); splitting tensile tests (ASTM C496: 2004, Abrishambaf *et al*. 2015); wedge splitting tests (Skocek and Stang 2008), and round panel tests (Minelli and Plizzari 2015, Salehian 2014). Amongst all the indirect tensile test methods for evaluating the $\sigma - w$ relationship of SFRC, the majority of the tests within the literature have been conducted on flexural prismatic specimens tested either under three (EN14651-5, ASTM C1609/C1609M-07, RILEM TC 162 TDF) or four -point (UNI 11039, JSCE SF4) bending. Most of the researchers prefer to perform the bending test due to the easiness of manufacturing the SFRC prismatic specimens and performing the flexural test (di Prisco *et al*. 2009). Several researchers (Zhang and Stang 1998, Planas *et al*. 1999, de Oliveira e Sousa *et al*. 2002, Barros *et al*. 2005, di Prisco *et al*. 2009) have attempted to develop a reliable approach to evaluate the post-cracking response of SFRC based on the data obtained from flexural test. This methodology is already incorporated in *fib* Model Code for Concrete Structures 2010 (hereafter abbreviated by "MC2010"). According to MC2010, the post-cracking $\sigma - w$ law of SFRC is defined by means of the experimental residual flexural strengths, f_{Rj} (j = 1 - 4), based on the load (P_j) corresponding to a crack mouth opening displacement (CMOD$_j$) obtained from flexural response (see Fig. 1a). In accordance with MC2010, the post-cracking design law that correlates the residual post-cracking $\sigma - w$ relationship can be defined using the parameters of serviceability residual strength, f_{Fts}, and ultimate residual strength, f_{Ftu}, as shown in Fig.1b. However, in accordance to the literature, it seems that MC2010 approach might overestimate the residual tensile strength of SFRC (Amin *et al*. 2015, Soltanzadeh *et al*. 2016a). Recently, Amin *et al*. (2015) proposed a simplified model to define the post-cracking residual relationship of SFRC for design purposes. Their model attempts to improve the accuracy of the SFRC post-cracking relationship proposed by the MC2010. Therefore, the latter authors suggest adopting the residual strength corresponding to CMOD$_2$ and CMOD$_4$ instead of CMOD$_1$ and CMOD$_3$, respectively, which are recommended by MC2010. The appropriate selection of the key sampling points (i.e. CMOD$_2$ and CMOD$_4$) provides a more reasonable modelling by covering the most important region of the $\sigma - w$ curve for both service and ultimate limit states design (Amin *et al*. 2015).

Evaluation of the characteristic values of SFRC tensile properties using MC2010 model, evidences that these characteristic values are remarkably lower than the average ones, due to the high scatter of the experimental results (Minelli and Plizzari, 2015). The scatter in the results can be mainly attributed to the use of notched prisms for the bending test and to a small fracture area in prismatic specimens. The notched specimens are often used due to the simplicity of the crack opening measurement during the flexural test. In this test set-up, the crack is forced to localize along the notch in a predefined fracture plane, which may not be the weakest cross section of the specimen. Therefore, the notch significantly influences the response of the SFRC bending specimen (Prisco *et al*. 2009) and increases the scatter of the SFRC post-cracking response depending on the variability of fiber spacing and orientation within the matrix (Amin *et al*. 2017). The small area of the fracture plane in prismatic specimens for flexural tests, ranging from 160 to 190 cm^2 (Minelli and Plizzari, 2015), can be another factor contributing to a larger scatter of the SFRC post-cracking response, especially in the case of concrete with a low volume fraction of fibers. This scatter, at the material level, may significantly influence the adopted characteristic values for design purpose and therefore, reduce the possibilities of designing cost competitive SFRC structures (Minelli and Plizzari, 2015).

According to Salehian *et al*. (2014), when comparing the experimental and numerical responses of self-compacting SFRC slab and shell elements under flexural loading, it is evidenced that for an accurate prediction of the structural behavior, a proper methodology for ascertaining the $\sigma - w$ relationship should be selected. This relationship should be capable to represent the post-cracking behavior of SFRC within this type of structures (i.e. slab and shell elements). The reason is that the orientation of fibers in self-compacting SFRC slabs and shell type structures is mostly orthogonal to the flux lines and the fiber structure has predominantly a 2D profile orientation (Abrishambaf *et al*. 2013). On the other hand, in prismatic elements, like the specimens produced for performing bending tests, the fibers are preferentially aligned along the longitudinal length of the element due to both the reorientation of the fibers due to the self-compacting concrete flow and the wall effects that occur during casting (Stähli 2008, Soltanzadeh *et al*. 2016b, Mazaheripour *et al*. 2016). This fiber alignment along the longitudinal axis of the prismatic elements, hence perpendicular to the fracture plane, leads to the overestimation of the post-cracking residual strengths for two-dimensional elements such as slabs and shells. Thus, ASTM C-1550 (2010) standard recommends to employ a statically round determinate panel (RDP) test, supported in three pivots at 120º, as an alternative to the direct tensile and prism bending tests. The required specimen for performing this test is a round shape panel of 800 mm diameter and 75 mm thick, with an approximately weight of 91 kg. This test has shown a higher repeatability of the results, consequently with a lower scatter when compared to the results obtained from prismatic bending tests (Minelli and Plizzari 2011, Bernard 2000), since when loading the RDP more and larger fracture surfaces are formed in the SFRC specimen (Amin *et al*. 2017). However, the large size of the specimen holds a major drawback both for handling and placing the RDP specimen on the testing rig (Minelli and Plizzari, 2015). To face up with these drawbacks, Minelli and Plizzari (2011) proposed a smaller round determinate panel (SRDP) with 600 mm diameter, 60 mm thickness with an approximate weight of 40 kg. An extensive experimental study on more than 50 SRDP specimens (Minelli F and Plizzari, 2011) has shown that the proposed geometry does not affect the results' scatter when compared to the one obtained by testing the classical RDP recommended by ASTM C-1550 standard. Hence, the SRDP test can be used instead of the RDP test to characterize the biaxial flexural capacity of SFRC (Minelli and Plizzari, 2015). However, none of the abovementioned methods can provide explicit information about the mechanical properties of SFRC, e.g. toughness indexes and post-cracking residual strengths, which can be derived directly from the prismatic bending test. Hence, a complementary model must be used to analyze the results obtained by these test setups and evaluate the mechanical properties of the SFRC. Recently, Mineli and Plizzari (2015) have proposed an analytical model, which was adapted from the MC2010 approach for tension softening materials, to derive a simplified $\sigma - w$ law for SFRC. This approach evaluates the post-cracking response of SFRC based on the experimental results of the SRDP test (i.e. load-deflection response and the width of the three radial cracks propagated during testing the round determinate panel, *w*). Then, the model defines an analytical relationship between crack tip opening displacement (CTOD) (by measuring the *w* for the three radial cracks during SRDP test), and CMOD (by assuming the given values of 0.5, 1.5, 2.5 and 3.5 for $CMOD_j$ according to MC2010). Based on the proposed methodology, the residual post-cracking strengths, f_{Rj}, can be derived by considering the results of the SRDP test in the same way as for the prismatic bending test suggested by MC2010 accordingly to EN14651 standard. After calculating the f_{Rj} residual strengths for the corresponding w_j, a uniaxial $\sigma - w$ can be determined for design purposes in accordance with MC2010.

Despite a vast research on application of three-point prism bending test and some research on using SRDPs for the characterization of SFRC, there is still limited research emphasizing the importance of employing an appropriate test typology to characterize SFRC for a safe design of structural element, mainly when SFRC has a pronounced self-compacting character. In the present research, several prismatic and SRDP specimens were cast using the same batch of SFRSCC. The specimens were tested to evaluate indirectly the post-cracking response of the SFRSCC. The aim of this study is to critically discuss all the advantages and disadvantages of using each of the two test methods (i.e. prism bending test and SRDP test), by means of comparing the different scatters that each of the tests produces.

On the other hand, to design SFRC structures accurately, reliable approaches should be used for estimating the $\sigma - w$ relationship that characterizes the post-cracking behaviour of a SFRC. Based on these experimental results obtained in the present study, the $\sigma - w$ relationship of the SFRSCC was assessed by means of different analytical / numerical approaches, as well as by the finite element method. The accuracy of the $\sigma - w$ responses obtained from the distinct approaches was evaluated and discussed.

2. Experimental Program

2.1. Concrete composition

In the present study, a steel fiber reinforced self-compacting concrete (SFRSCC) comprising 90 kg/m^3 (corresponding to a volume fraction, V_f , of 1.15%) of hooked end steel fibers was developed for fabricating all the specimens. The methodology adopted to design the concrete composition has followed three stages (Soltanzadeh *et al*. 2015). Firstly, the proportion of constituents for attaining an optimized paste was defined. Then, the optimum volume percentage of each type of aggregates regarding the granular skeleton of the concrete was assessed. Finally, the optimum correlation between the paste and the solid skeleton was defined in order attain adequate self-compacting characteristics.

The SFRSCC was produced using Portland cement CEM I 42.5R, fly ash class F, a third-generation superplasticizer based on polycarboxylate ether (PCE) polymers (Glenium SKY 617), tap water, four types of aggregates (containing fine and coarse river sand, respectively, with maximum size of 2.4 mm and 4.8 mm; as well as two types of crushed granite with 9 mm and 12.5 mm maximum size, respectively). The hooked steel fibers used in the mix were 33 mm in length, l_f , with an aspect ratio (length to diameter ratio, l_f / d_f) of 65, and a tensile strength of 1100 MPa.

Table 1 presents the developed SFRSCC composition. The flowability of the SFRSCC was evaluated by means of the slump-flow test (BS EN 12350-8) at the fresh state. During this test, the time to reach the spread diameter of 500 mm was measured as 3.5 sec (T_{50}) and finally, the concrete reached to a total spread diameter of 650 mm. Although the Abrams cone was always used in the inverted position for evaluating the slump flow, the developed concrete presented a good homogeneity, without any sign of segregation. This can be attributed to the application of optimum amount of fly ash (besides using the superplasticizer), which is a pozzolanic material that acts as micro-rollers, and significantly decrease the friction and the flow resistance of the paste (Soltanzadeh *et al*. 2018).

2.2. Mechanical characterization of the SFRSCC

The mechanical behavior of the SFRSCC was assessed through distinct experimental tests, such as the Young's modulus test (BS EN 12390–13), compressive strength (ASTM C39/C39M-14) and flexural tests (EN14651). The average values of Young's modulus and compressive strength of the SFRSCC were E_{cm} = 34.13 GPa (CoV = 0.69%) and f_{cm} = 61.67 MPa (CoV = 2.4%) at the ages of 28 days, respectively. These properties were assessed on three cylindrical specimens with 150 mm diameter and 300 mm height. The characteristic compressive strength, f_{ck} , of concrete was 54 MPa. Based on the obtained experimental results, the average tensile strength of the SFRSCC was determined as 3.9 MPa, using the following equation proposed by MC2010:

$$f_{ct} = \begin{cases} 0.3 f_{ck}^{2/3} & \text{for} \le C50 \quad (a) \\ 2.12 \ln(1 + f_{cm}/10) & \text{for} > C50 \quad (b) \end{cases} \tag{1}$$

The post-cracking response of the SFRSCC was characterized by executing flexural tests on six prismatic specimens and nine SRDP specimens. The detailed description of the test setup and the obtained results are presented in the two following sections (Sec. 2.2.1 and 2.2.2).

2.2.1 Prism bending test and results

One of the test methods applied to characterize the post-cracking response of the SFRSCC was the three-point bending test, which was conducted on six notched beams of 150 × 150 mm^2 cross section and 600 mm length, following the recommendations of EN14651. The test was carried out in close-loop displacement control using a vertical linear variable differential transformer, LVDT, installed at the mid-span of the specimen. A displacement rate of 1 μm/s at the mid-span of the specimens was adopted up to a deflection of 0.1 mm to avoid instability at the first phase of the crack formation and propagation. After reaching to the deflection of 0.1 mm, the rate of displacement was increased to 3 μm/s and kept constant up to the failure of the prisms. The CMOD of the specimens was recorded using a LVDT, positioned across the notch of the specimen at the bottom surface of the prism.

Fig. 2 depicts the post-cracking response of the SFRSCC in terms of nominal flexural stress versus CMOD relationship, abbreviated hereafter by $\sigma_N - w$ relationship. From these responses, the stress at the limit of proportionality, $f_{ct,L}^{f}$, (corresponding to the maximum load reached within a CMOD of 0.05 mm) and the residual flexural tensile strengths of the SFRSCC, f_{R1} to f_{R4}, corresponding to distinct values of CMOD, were obtained as indicated in Table 2. In accordance with MC2010, the toughness class of this concrete is ‘‘8a” (f_{R3k} / f_{R1k} = 0.63).

2.2.2 Small round determinate panel (SRDP) test and results

The SRDP tests were performed on nine round specimens of 600 mm diameter and 60 mm thickness in accordance with the specimen size and the test setup proposed by Minelli and Plizzari (2011) to evaluate the post-cracking response of fiber reinforced concretes. Fig. 3 shows the general configuration of the SRDP and the arrangement of the test setup. During the test, the panels were simply supported on three symmetrically arranged pivot points, disposed at 120° around the specimen. A round steel transfer plate of 50 mm diameter and 25 mm thick was used to support the SRDP on the pivots. The transfer plates had a spherical seat of about 6 mm depth, which was machined into the surface to achieve the ball connection as suggested by ASTM C1550-05 (see Fig. 3a and 3b). Teflon sheets covered these transfer plates to mitigate the effect of the support’s friction on the behavior of the SRDPs, as recommended in Frazão *et al.* 2018.

The SRDPs were loaded at the center and the specimen’s central deflection was measured using a LVDT installed vertically beneath the specimens. Three additional LVDTs were also used for measuring the three main cracks, initiated at the bottom of the panels. These LVDTs were horizontally installed at a radial distance of 120 mm from the center point of the panels, as shown in Fig. 3c.

The test procedure was controlled using a LVDT of 50 mm gauge length that measured the vertical deflection of the loading plate. The imposed deflection rate was 0.25 mm/min up to the deflection of 0.5 mm, and thereafter, the rate of deflection was increased to 1.0 mm/min up to failure of the specimens.

By loading each of the specimens, cracks appeared on the bottom surface of the specimen. These cracks initiated from the central point of the panel. They developed gradually to the edge of the panel and were located, in general, between consecutive supports. All the specimens have failed in flexure. Fig. 4 shows the crack pattern of the tested specimens. A large number of secondary cracks were developed from the main cracks. In some panels was observed the deviation of the cracks from the bisector of the segments, which can be attributed to the inhomogeneous dispersion and orientation of fibers in the panels, which is also dependent on the casting procedure (Hu *et al*. 2018). Fig. 5 depicts the load vs. central deflection relationship obtained by testing the SRDPs. This figure shows that the crack was initiated at the average load of 17.5 kN. The average peak load of 27 kN has occurred at a central deflection of 1.4 mm. Beyond the peak point, the load decreases with the opening of the formed cracks and a deflection softening response was observed.

3. Evaluation of σ - *w* relationship of the developed SFRSCC

3.1 Analytical approaches

Based on the experimental results presented in previous sections, the tensile stress vs. crack mouth opening displacement relationship, $\sigma - w$, of the SFRSCC was evaluated according to three distinct analytical approaches available in literature, namely: MC2010, as well as the formulation proposed by Amin *et al*. (2015) and Minelli and Plizzari (2015).

In general, the behavior of fiber reinforced composites in tension prior to cracking is defined by a stress – strain response, $\sigma - \varepsilon$. After micro cracking coalesces into a macro crack, a $\sigma - w$ relationship describes better the behavior of the reinforced concrete. Fig. 6 shows the contribution of both fibers and matrix to the tensile post-cracking behavior of SFRC. In the following sections, (Sec. 3.1.1 to 3.1.3) the method for evaluating the $\sigma - w$ relationship in accordance with each of the three abovementioned analytical approaches (i.e. MC2010, Amin *et al*. 2015, and Minelli and Plizzari 2015) is introduced.

3.1.1 Stress vs. crack width relationship based on the MC2010

The MC2010 guidelines proposes a stress vs. crack width constitutive law for strain softening fiber reinforced concretes, as already introduced in Fig. 1b. This constitutive law is defined based on the values of the residual flexure strengths, f_{R1} and f_{R3}, corresponding to the values of CMOD of 0.5 and 2.5 mm, respectively (see Fig.1a). The residual flexural strengths are calculated according to the following equation (by using the results of prism bending test):

$$f_{Rj} = (3P_j.l)/(2bh_{sp}^2) \tag{2}$$

where, P_j is the load corresponding to $CMOD_j$, l is the span length of the prismatic specimen, and b and h_{sp} are respectively the width of the specimen and the distance between the tip of the notch and top of the specimen. The f_{Fts} and ultimate residual strength, f_{Ftu}, used for defining the $\sigma - w$ shown in Fig. 1b, are obtained from:

$$f_{Fts} = 0.45.f_{R1} \tag{3}$$

$$f_{Ftu} = f_{Fts} - (w_u / CMOD_3).(f_{Fts} - 0.5 f_{R3} + 0.2 f_{R1}) \tag{4}$$

where, w_u is the maximum value of the crack width, which generally is accepted as w_u = $CMOD_3$ = 2.5 mm for FRC elements failing in bending.

3.1.2 Stress vs. crack width relationship based on the model of Amin *et al*. (2015)

In the approach proposed by Amin *et al*. (2015), likewise the one recommended by MC2010 guideline, the experimental bending test results are used to derive a simplified $\sigma - w$ relationship for strain softening SFRC. In accordance with this approach, the stress for a certain crack width, $\sigma(w)$, is calculated as follows:

$$\sigma(w) = \sigma_c(w) + \sigma_f(w) \tag{5}$$

where $\sigma_c(w)$ and $\sigma_f(w)$ are the nominal stress carried out by the contribution of concrete and fibers, respectively. The contribution of the matrix component to the stress carrying capacity is more considerable at the early post-cracking stages. This contribution swiftly reduces and becomes negligible when increasing the moment and CMOD at later stages of the cracking process. Fig. 6 illustrates this response. According to the proposal of Amin *et al*. (2015), the contribution of plain concrete to the tensile stress – crack width relationship is calculated as follow:

$$\sigma_c(w) = \mathrm{c}_1 . f_{ct} . e^{-c_2 w} \tag{6}$$

where f_{ct} is the tensile strength of plain concrete, c_1 is a coefficient, which is assumed as unity for Mode I fracture, and the coefficient c_2 is calculated as follows:

$c_2 = 30/(1+100V_f)$	For mortar and concrete with a maximum aggregate size lower than 10 mm.	(7a)
$c_2 = 20/(1+100V_f)$	For mortar and concrete with a maximum aggregate size higher than 10 mm.	(7b)

In the design approach proposed by Amin *et al*. (2015), the $\sigma - w$ relationship of SFRC is evaluated based on the residual flexural strengths f_{R2} and f_{R4}, corresponding to a CMOD of 1.5 and 3.5 mm, instead of the ones proposed by MC2010 (i.e. f_{R1} and f_{R3}). In this simplified model, it is assumed that the neutral axis is sufficiently high in the section due to significant cracking and thus the contribution of the matrix can be neglected when compared to the fiber contribution. Therefore, $CMOD_2$ and $CMOD_4$ are selected for evaluating the post-cracking response of SFRC, since these two CMODs are sufficiently distant from the initial cracking stage.

In accordance with this approach, the crack width, *w*, and stress due to the fiber contribution, σ_f, are calculated accordingly to Eq. (8) and Eq. (9), respectively.

$$w = (\mathrm{CMOD}\ .\ 0.35h_{sp})/(D - 0.3h_{sp}) \tag{8}$$

where *D* is the total depth of the prismatic specimen (150 mm).

$$\sigma_f = (f_{R2}/3) + (f_{R4} - f_{R2})\xi(\mathrm{w}) \geq 0 \tag{9}$$

where f_{R4} and f_{R2} are obtained from Eq. (2), and $\xi(\mathrm{w})$ is calculated as follow:

$$\xi(\mathrm{w}) = (w/3).(D-d_n)/(h_{sp}-d_n) - 1/4 \tag{10}$$

where, d_n is the depth of neutral axis in the prismatic specimen. Amin *et al.* 2015 propose a conservative value of $d_n = 0.3\ h_{sp}$ in the simplified model for design purposes.

3.1.3 Stress vs. crack width relationship based on the model of Minelli and Plizzari (2015)

The last analytical model employed in the present study to evaluate the post-cracking behavior of SFRC is the one proposed by Minelli and Plizzari (2015). This model adopts the results obtained in SRDP tests for deriving a simplified $\sigma - w$ relationship for strain-softening SFRC. The $\sigma - w$ law can be defined also based on the concept of the residual flexural strengths, f_{Rj} . However, they are now calculated using the results of the SRDP test.
The method proposes an analytical relation between the width of the cracks, w_j (j = 1 to 4), in the SRDP, which are measured during the test, and the four values of $\mathrm{CMOD_j}$ (i.e. 0.5, 1.5, 2.5 and 3.5 mm) obtained from the three-point bending tests according to the EN14651 standard. This w_j - $\mathrm{CMOD_j}$ relationship is defined for the SRDP as follows:

$$w_j = 0.768\ \mathrm{CMOD}_j \tag{11}$$

Then, the load F_j (j = 1 to 4), corresponding to the calculated values of w_j can be evaluated based on the experimental results of testing the SRDPs. A typical $F_j - w_j$ diagram from a fiber reinforced SRDP test is represented in Fig. 7. Finally, the residual post-cracking strengths can be obtained using Eq. (12).

$$f_{Rj} = (0.00186\, F_j\, D')/\mathrm{t}^2 \tag{12}$$

where D' is the effective diameter of the SRDP (it is considered as 550 mm for the tested SRDPs), and t is the thickness of SRDP.

By having the pairs of w_j and f_{Rj}, the $\sigma - w$ diagram is determined in accordance with MC2010 as described in section 3.1.1.
Fig. 8a represents the nominal flexural stress *vs.* CMOD relationship of the SFRSCC of the SRDPs, calculated applying Eq. (11) and Eq. (12) to the data obtained in these tests. From a crack opening registered in the SRDP, w_i, (i representing the scan readings registered in the experimental tests) the correlated CMOD is determined from Eq. (11), $CMOD_i$, and the corresponding nominal flexural stress from Eq. (12), σ_{Ni}, constituting the point $\sigma_{Ni} - CMOD_i$ of this relationship. The coefficient of variation, as an indicator of the scatter of the test result, was calculated for the residual strength of SFRSCC obtained based on the two test typologies (i.e. prism bending test

and SRDP test), at different CMODs, and the determined results are shown in Fig. 8b. These results demonstrate that by using the SRDP test, a lower coefficient of variation was obtained for the residual strength of SFRSCC at any CMOD. This can be attributed to the larger fracture area of SRDPs (compared to that of prismatic specimens), thus with a high number of fibers bridging the cracks.

Although the results indicate that a higher accuracy on the evaluation of the residual strength of SFRSCC can be obtained by determining this data from SRDP test, further work in this respect should be done by executing a relatively large, but of same number, beam and SRDP tests.

In case of the SRDP tests, the tendency is to form three cracks, but the impossibility of assuring a homogeneous fibre distribution and orientation can lead to the formation of a smaller or higher number cracks than the expected value, which was the case occurred in the present experimental programme. In Fig. 8a is compared the $\sigma - CMOD$ relationship for the panels SRDP-1 and SRDP-2, where it was formed three and two failure cracks, respectively. It is observed that the panel with higher number of cracks has presented a larger post-cracking flexural capacity, in consequence of a larger fracture surface, thus with higher number of fibres resisting to the crack opening process.

3.1.4 Comparison of the $\sigma - w$ relationships obtained from distinct approaches

Fig. 9 depicts the $\sigma - w$ relationships obtained by the three presented approaches, namely, MC2010, Amin *et al*. (2015) and Minelli and Plizzari (2015) for the developed SFRSCC up to a crack width of 2.5 mm. It can be seen that the approaches proposed by Amin *et al*. (2015) and Minelli and Plizzari (2015) render close $\sigma - w$ relationships, whereas the relationship obtained by MC2010 provides higher residual tensile stresses, in particular for lower crack widths. The capability of these relationships (i.e. proposed by MC2010, Amin *et al*. 2015 and Minelli and Plizzari 2015) to estimate the SFRSCC mechanical behavior will be assessed in Sec. 4. The experimental load vs. deflection responses of SRDPs were simulated by adopting each constitutive relationship obtained from the distinct methodologies.

3.2 Assessment of the $\sigma - w$ by performing Inverse Analysis based on numerical strategies

In the present section, the $\sigma - w$ relationship of the developed SFRSCC was evaluated by applying two inverse analysis procedures to the experimental load vs. deflection responses of SRDP and the load - CMOD from three-point notched beam bending tests. For this purpose, the approach developed by Salehian *et al*. (2014) will be used for the SRDP, while a smeared cracking model available in the Finite Element software (FEMIX 4.0) will be adopted for the three-point notched beam bending tests.

3.2.1 Salehian *et al.* (2014) inverse analysis approach applied to small round determinate panel test

The behavior of the tested SRDPs was simulated by means of a numerical model developed by Salehian *et al.* (2014). This model is based on the application of the principle of virtual work where the internal virtual work is restricted to the moment-rotation occurred in the formed cracks while the external virtual work is due to the applied load to the panel. The model also considers the kinematics conditions due to the central deflection of the panel as a consequence of the cracks' rotations of the plates composing the cracked panel (Fig. 10). Finally, the model integrates constitutive laws for the SFRC in tension and compression for deriving the moment-rotation response governing the propagation process of the cracks in the panel, according to an approach developed by Barros *et al.* (2015).

The Salehian *et al*. 2014 model considers that the response of SRDPs is linear elastic up to cracking formation, assuming that the cracks radiate from the center of the panel (point C in Fig. 10) and propagate along straight lines. It is also assumed that a crack propagates between two consecutive supports, by dividing the SRDP into three rigid plates / sectors. The rotation of these rigid plates, due to crack opening, causes the vertical deflection of the central point of the panels, δ_c, as shown in Fig. 10a. Each rigid plate rotates around an axis. These axes are shown in Fig. 11b by using colorful lines (i.e. the axis is shown in purple line for plate 1, in pink line for plate 2 and in green line for plate 3). They are drawn tangent to the slab perimeter at the support points and intersect mutually at the assumed imaginary point located in the alignment of the median crack.

Each radial crack (propagating between two adjacent support points in each circle sector of the SRDP) can align with a certain deviation respect to the line bisecting the same sector (represented by blue lines in Fig. 10b). This misalignment of the i^{th} crack, which is shown as β_i in Fig. 10b, causes to form two corresponding rotational arms (i.e. $A_{i,1}B_{i,1}$ and $A_{i,2}B_{i,2}$) intersecting the crack alignment in two distinct points of $B_{i,1}$ and $B_{i,2}$. Then, the overall rotation of the i^{th} crack in the panel results from the rigid rotation of the two adjacent plates, named as plate 1 and plate 2, around their own axis. The model assumes a linear variation for the vertical deflection of the plates along the crack. It is also assumed that there is no deflection at the pivot of the i^{th} crack (P_i in Fig. 10b). Then, the deflection of the two points $B_{i,1}$ and $B_{i,2}$ can be calculated by considering the central deflection of the panel in the k^{th} step of loading (δ_c^k) as follow:

$$\delta_{Bi,1}^k = (B_{i,1}.P_i / CP_i).\delta_c^k \tag{13}$$

$$\delta_{Bi,2}^k = (B_{i,2}.P_i / CP_i).\delta_c^k \tag{14}$$

The deflection of the points $B_{i,1}$ and $B_{i,2}$ imposes the rotations of $\theta_{i,1}^k$ and $\theta_{i,2}^k$, respectively, as illustrated in Fig. 10b. These rotations can be calculated using the following equations:

$$\theta_{i,1}^k = \delta_{Bi,1}^k / (\mathrm{A}_{i,1}.\mathrm{B}_{i,1}) \tag{15}$$

$$\theta_{i,2}^k = \delta_{Bi,2}^k / (\mathrm{A}_{i,2}.\mathrm{B}_{i,2}) \tag{16}$$

Then, the rotation of i^{th} crack imposed from deflection "δ_c^k" is obtained as the summation of the rotation value of the two adjacent plates connecting the i^{th} crack (plate 1 and plate 2 in Fig. 10).

$$\theta_i^k = \theta_{i,1}^k + \theta_{i,2}^k \tag{17}$$

The resisting bending moment per unit width of the SRDP, M_i^k, is obtained from the imposed θ_i^k and considering the $\theta_i^k - M_i^k$ determined by using DOCROS software, where a cross section is decomposed in layers and for each layer a constitutive law is attributed to simulate the compression and tension behavior of the corresponding material (Varma, 2012). In fact, DOCROS determines a moment-curvature relationship for the cross section, but Eq. (18) is used to determine the rotation from the curvature assuming a crack bandwidth (Barros *et al.* 2005) equal to half of the panel's thickness according to the recommendations of RILEM TC TDF-162 (Vandewalle *et al.* 2002)

$$\theta_i^k = (t/2).\chi_i^k \tag{18}$$

To determine the $M_i^k - \chi_i^k$ relationship for the SRDP sections using DOCROS software, the cross section of the SRDP was discretized into 60 layers of 1 mm thick and 550 mm width. The compressive and uncracked tensile behavior of the SFRSCC was modelled with the stress - strain relationship suggested by MC2010, see Fig. 11a. The quadrilinear $\sigma - w$ relationship, schematically plotted in Fig. 11b, was considered for simulating the post-cracking tensile behavior of the SFRSCC. The $\sigma - w$ relationship of the SFRSCC was obtained by fitting the estimated force-deflection response to the one obtained experimentally (based on the inverse analysis method). After determining the $M_i^k - \chi_i^k$ response of the SRDPs, the moment – rotation relationship, $M_i^k - \theta_i^k$, of the SFRSCC panel can be obtained, in which the rotation (θ_i) is determined from Eq. (18)

Finally, the force corresponding to the deflection at the central point of the SRDP in the k^{th} loading step can be determined using Eq. 19 from the application of the principle of virtual work and assuming that the internal virtual work is restricted to the one carried out by the cracking process of the n_{cr} cracks at the panel (Salehian *et al.* 2014).

$$F_c^k = \frac{1}{\delta_c^k}\sum_{i=1}^{n_{cr}}(M_i^k \times L_{cr,i})\theta_i^k \tag{19}$$

where $L_{cr,i}$ is the length of the i^{th} crack (see Fig. 10b).

Fig.12 represents the flowchart of the method adopted for calculating the force - deflection $(F_c^k - \delta_c^k)$ relationship of the SRDPs.

3.2.2 Three-point notched beam bending test

The $\sigma - w$ relationship of the developed SFRSCC was also estimated using FEMIX 4.0 software. This is a computer code based on the Finite Element Method (FEM), whose description of its main features is available in Barros (2016), with a critical analysis on the debilities and potentialities of the type of model used in the present work, namely a multi-directional fixed smeared crack (MDFSC) model. The mode I crack propagation is simulated by the type of crack normal stress vs. crack normal strain, $\sigma_n^{cr} - \varepsilon_n^{cr}$, represented in Fig. 13 (quadrilinear diagram). Normalized strain, $\xi_i (i = 1, 2)$, and stress, $\alpha_i (i = 1, 2)$, parameters are used to define the transition points between linear segments, being G_f^I the fracture energy mode I, while l_b is the characteristic length (crack bandwidth) used to assure that the numerical results are not dependent of the finite element mesh refinement. The version of the MDFSC model adopted in the present simulations assumes a linear elastic behavior in compression of the concrete (Ventura-Gouveia 2011).

In the present study, the mode I fracture parameters and, consequently, the $\sigma - w$ relationship were assessed by an inverse analysis (IA) procedure of the prismatic bending test results. Fig. 13 depicts the adopted quadrilinear $\sigma - w$ diagram used in the IA. An exhaustive search procedure was employed during IA to assess parameters ξ_i and α_i (i = 1–3), the tensile strength, f_{ct}, and the fracture energy, G_f^I, which minimize the ratio between the area underneath the experimental load - deflection curve and the numerical one.

The numerical load-deflection response of SFRSCC prismatic specimen was obtained considering the specimen's geometry, loading and support conditions in agreement with the experimental prismatic bending test setup. Fig. 14a shows the finite element (FE) mesh geometry. Linear plane stress finite elements of four nodes were adopted. A Gauss-Legendre integration scheme of 2 × 2 *IP* was adopted. To assure the formation of a single crack plane along the specimen symmetry plane, a Gauss-Legendre integration scheme of 2 × 1 *IP* was adopted for the elements located above the notch. Apart these elements, i.e. located above the notch, where cracked behavior in tension was assumed, a linear elastic material behavior was assigned to all the remaining elements. Table 3 shows the parameters ξ_i, α_i, f_{ct} and G_f^I, obtained from the inverse analysis. The corresponding numerical flexural stress *vs*. CMOD response of the SFRSCC prismatic specimens is compared with the experimental results in Fig. 14b as well. This comparison verifies that a good agreement was obtained between the experimental and numerical load – deflection curves.

4. Predictive performance of the distinct methods for derivation of the σ – w law

The predictive performance of the three abovementioned approaches, proposed by MC2010, Amin *et al.* (2015) and Minelli and Plizzari (2015), which were adopted for deriving the $\sigma - w$ relationship of strain-softening SFRSCC, was assessed by simulating the experimental force – deflection response of the SRDPs obtained from the experimental tests. For this purpose, these relationships were used with the numerical model of Salehian *et al.* (2014) and assuming the geometric configuration of the cracks observed in the tested SRDPs, as shown in Fig. 15. The cracks were assumed as straight lines, in order to be in agreement with the assumptions of the Salehian *et al.* (2014) model. In addition, the compressive strength and elastic modulus of the SFRSCC were defined in accordance with the test results presented in Sec. 2.2, while the $M_j^k - \theta_j^k$ response of SFRSCC was obtained using DOCROS software, as explained previously (see Se. 3.2.1). Fig.16 compares the average $F_c^k - \delta_c^k$ relationship obtained from the SRDP tests with the envelope of the simulations by taking into account the distinct crack patterns observed on the tested panels. The three approaches have predicted with good level of accuracy the $F_c^k - \delta_c^k$ relationship registered experimentally, but those based on the Minelli and Plizzari (2015) recommendations and from DOCROS predicted better the full experimental response. The σ – w relationship obtained from Amin *et al.* (2017) approach was also capable of capturing well the peak load, however a rather conservative estimation of the post-peak response was obtained, i.e. for central displacements higher than 1.5 mm. On the other hand, the MC2010 constitutive law has provided an unsafe estimate of the experimental average peak load, but quite accurate predictions in the softening stage, mainly for deflections within the range of 3 and 6 mm.

The residual tensile stresses obtained at four key sampling points, respectively, w = 0.5, 1, 2, and 2.5 mm, by means of the two numerical methods (i.e. Salehian *et al.* (2014) and IA in FEM), as well the three analytical approaches (i.e. MC2010, Amin *et al.* 2015, Minelli and Plizzari 2015) are presented in Table 4. The table shows that the higher residual stresses were estimated using FEMIX software and the MC2020 approach, since these two methods were both supported on the determination of the post-cracking behavior from the three-point bending tests of the prismatic specimens. On the other hand, residual stresses computed with the analytical approach of Salehian *et al.* (2014) rendered closer results to the ones obtained with the method of Minelli and Plizzari (2015), since these two approaches are based on the round determinate panel test results.

5. Conclusions

In order to design cost-effective SFRC structural elements, it is important to define accurately the post-cracking tensile behavior of SFRC. The post-cracking response of SFRC can be tested directly using uniaxial tensile test or it can be obtained indirectly through inverse analysis of a notched prismatic specimen or a SRDP tested in bending. The indirect methods for estimating the SFRC constitutive laws are quite attractive due to the ease of manufacturing the required specimens and performing the tests. In this regard, there are several analytical and numerical methods available for estimating indirectly the $\sigma - w$ relation of the fiber reinforced concrete, FRC, based on the obtained experimental results. The present study attempts to evaluate the accuracy of several available methodologies for ascertaining the FRC tensile constitutive laws. To this aim, a SFRSCC with 90 kg/m^3 of steel fibers was developed and its behavior experimentally assessed. The present experimental program comprised the fabrication and testing of nine SRDPs (smaller round determinate panels) as well as six notched prismatic specimens. The post-cracking response of the developed SFRSCC was then estimated using two numerical approaches, namely FEM-based and Salehian *et al.* (2014), as well as three analytical approaches: MC2010, and those suggested by Amin *et al.* (2015) and Minelli and Plizzari (2015). The reliability of the estimated stress – crack width, $\sigma - w$, relationship by these methods was evaluated by using a numerical model to predict the force-deflection response of SRDPs. The accuracy of the SFRSCC post-cracking response estimated using different approaches was then evaluated by comparing the load – deflection relationship predicted numerically to the corresponding one obtained experimentally. From the present study the following conclusions can be drawn:

- When comparing the results obtained by testing the SFRSCC prism and SRDP specimens, it was observed a higher scatter of the results when executing the prism bending test. This higher dispersion of the results can be attributed to the use of notched prisms for the bending test and the smaller fracture area in the prismatic specimens. By application of SRDP test, the post-cracking response of the SFRC can be evaluated with a higher accuracy degree.
- The constitutive laws estimated by all the numerical and analytical approaches were acceptable for design purposes. These constitutive laws can be applied in the simplified approaches of deformation analysis of concrete members reinforced with fibers and bars.
- All the numerical and analytical approaches demonstrated an acceptable accuracy for the evaluation of the post-cracking behavior of SFRC. However, the prediction of the load – deflection relationship of the

SRDPs obtained with the relationships from the methodology proposed by Minelli and Plizzari (2015) was the most accurate.

- From adopting the relationships obtained by the Amin et al. (2015) methodology, it was possible to accurately estimate the load-deflection response of SRDPs up to a central displacement of 1.5 mm, whereas when using the constitutive laws proposed by MC2010 lead to an underestimation of both the peak load and the residual response (up to a central displacement of 3 mm).

Acknowledgements

The authors acknowledge the support provided by FEDER funds through the Operational Programme for Competitiveness and Internationalization - COMPETE and by national funds through FCT (Portuguese Foundation for Science and Technology) within the scope of the project InOlicTower, POCI-01-0145-FEDER-016905 (PTDC/ECM-EST/2635/2014).

References

Abrishambaf A, Barros J.A.O, Cunha V. Tensile stress-crack width law for steel fibre reinforced self- compacting concrete obtained from indirect (splitting) tensile tests. Cem Concr Compos J 2015; 57: 153-165.

Abrishambaf A, Barros J.A.O, Cunha V. Relation between fibre distribution and post-cracking behaviour in steel fibre reinforced self-compacting concrete panels. Cem Concr Research J 2013; 51: 57-66.

Amin A, Foster S.J, Gilbert R.I, Kaufmann W. Material characterisation of macro synthetic fibre reinforced concrete. Cem Concr Compos J 2017; 84: 124-133.

Amin A, Foster S.J, Muttoni A. Derivation of the σ-w relationship for SFRC from prism bending tests. Struct Concr 2015; 93-105.

ASTM C1550-10. Standard test method for flexural toughness of fiber reinforced concrete (using centrally loaded round panel). West Conshohocken (PA): ASTM International; 2010.

ASTM Standard C1609/C1609M-07. Standard test method for flexural performance of fiber-reinforced concrete (using beam with third-point loading). West Conshohocken (PA): ASTM International; 2010.

ASTM C39/C39M-14. Standard test method for compressive strength of cylindrical concrete specimens. Annual Book of ASTM Standard, Am Soc Test Mater 2014. doi: http://dx.doi.org/10.1520/C0039M-14A.

ASTM C496, Standard test method for splitting tensile strength of cylindrical concrete specimens, Annual Book of ASTM Standards: American Society of Testing Materials, 2004.

Barros J.A.O. Debilities and strengths of FEM-based constitutive models for the material nonlinear analysis of steel fiber reinforced concrete structures. Proceedings of the 9th International Conference on Fracture Mechanics of Concrete and Concrete Structures, FraMCoS-9, V. Saouma, J. Bolander and E. Landis (Eds), California, May 29-June 1, 2016.

Barros J.A.O, Cunha V.M.C.F, Ribeiro A.F, Antunes J.A.B. Post-Cracking Behaviour of Steel Fibre Reinforced Concrete, Mater. Struct. J 2005; 38(275) : 47-56. doi: 10.1617/14058.

Barros J.A.O., Foster S. An integrated approach for predicting the shear capacity of fibre reinforced concrete beams. Eng Struct J 2018; (174): 346-357.

Barros J.A.O., Taheri M., Salehian H. A model to simulate the moment-rotation and crack width of FRC members reinforced with longitudinal bars. Eng Struct J 2015; 100: 43-56.

Bernard E.S. Behaviour of round steel fiber reinforced concrete panels under point loads, Mater. Struct J 2000; (33) : 181-188.

BS EN 12350-8. Testing fresh concrete. Self-compacting concrete. Slump-flow test. 2010.

BS EN 12390–13. Testing hardened concrete-Part 13: determination of secant modulus of elasticity in compression; 2014.

Cuenca E, Serna P. Shear behavior of prestressed concrete beams made of self-compacting fiber reinforced concrete. J Constr Build Mater 2013; 45:145-56.

Cunha V. Steel Fibre Reinforced Self-Compacting Concrete (from Micro-Mechanics to Composite Behaviour) [Doctoral thesis]. Portugal: University of Minho; 2010.

de Oliveira e Sousa, J. L. A., Gettu, R., Barragán, B. E.: In- verse analysis of the notched beam response for determining the σ-w curve for plain and fiber reinforced concretes. Anales de Mecánica de la Fractura, 19, 2002, pp. 393–398.

di Prisco M, Colombo M, Dozio D. Fibre-reinforced concrete in fib Model Code 2010: principles, models and test validation, J Struct Concr 2013; (14): 342-361.

di Prisco M, Plizzari G, Vandewalle L. Fibre reinforced concrete: new design perspectives, J Mater Struct 2009; (42) : 1261-1281.

EN14651. Precast concrete products – test method for metallic fiber concrete – measuring the flexural tensile strength. Belgium: Europ. Standard, Brussels; 2005.

fib – International Federation for Structural Concrete. fib Model Code for Concrete Structures 2010. Berlin: Verlag Ernst & Sohn, 2013.

Frazão C.M.V., Barros J.A.O., Bogas J, Pilakoutas K. An experimental investigation on the post-cracking behaviour of Recycled Steel Fibre Reinforced Concrete. FRC2018: Fibre Reinforced Concrete: from Design to Structural Application, Joint ACI-fib-RILEM International Workshop, Brescia, June 2018.

Soltanzadeh, F., Mazaheripour, H., Barros, J., Taheri, M., Cruz, J.S. Experimental study on shear behavior of HPFRC beams reinforced by hybrid pre-stressed GFRP and steel bars. Proceedings of the 7th International Conference on FRP Composites in Civil Engineering, CICE 2014.

Hu Hang, Papastergiou Panos, Angelakopoulos Harris, Guadagnini Maurizio, Pilakoutas Kypros. Mechanical properties of SFRC using blended manufactured and recycled tyre steel fibres. J Const Build Mater 2018; (163): 376–389.

Mazaheripour, H., Barros, J.A.O., Soltanzadeh, F., Sena-Cruz, J. Deflection and cracking behavior of SFRSCC beams reinforced with hybrid prestressed GFRP and steel reinforcements. J Eng Struct 2016; (125):546-565.

Minelli F, Plizzari GA. A new round panel test for the characterization of fiber reinforced concrete: a broad experimental study. ASTM J Test Eval 2011;39(5):889–97 [ISSN:1945-7553].

Minelli F, Plizzari GA. Derivation of a simplified stress–crack width law for Fiber Reinforced Concrete through a revised round panel test. J Cem Concr Comp 2015; (58): 95–104.

Planas J, Guinea GV, Elices M. Size effect and inverse analysis in concrete fracture. Journal of Fracture1999; (95): 367–378.

Salehian Hamidreza, Barros Joaquim A.O., Taheri Mahsa. Evaluation of the influence of post-cracking response of steel fibre reinforced concrete (SFRC) on load carrying capacity of SFRC panels. J Const Build Mater 2014; (73): 289-304.

Skocek J, Stang H. Inverse analysis of the wedge-splitting test. J Eng Fract Mech 2008; (75): 3173-3188.

Soltanzadeh F, Barros JAO, Santos RFC. High performance fiber reinforced concrete for the shear reinforcement: experimental and numerical research. J Constr Build Mater 2015; (77): 94-109.

Soltanzadeh F, Edalat-Behbahani A, Mazaheripour H, Barros JAO. Shear resistance of SFRSCC short-span beams without transversal reinforcements. J Compos Struct 2016a; (139):42-61.

Soltanzadeh F, Edalat-Behbahani A, Barros JAO, Mazaheripour H. Effect of fiber dosage and prestress level on shear behavior of hybrid GFRP-steel reinforced concrete I-shape beams without stirrups. J Compos Part B 2016b; (102): 57-77.

Soltanzadeh F, Emam-Jomeh M, Edalat-Behbahani A, Soltan-Zadeh Z. Development and characterization of blended cements containing seashell powder. J Constr Build Mater 2018; (161): 292–304.

Soltanzadeh, F., Mazaheripour, H., Barros, J., Taheri, M., Cruz, J.S. Experimental study on shear behavior of HPFRC beams reinforced by hybrid pre-stressed GFRP and steel bars. Proceedings of the 7th International Conference on FRP Composites in Civil Engineering, CICE 2014.

Stähli, P. Ultra-fluid, oriented hybrid-fibre-concrete [Doctoral thesis]. Diss. ETH No. 17996, ETH Zurich, 2008.

UNI 11039, Steel fiber reinforced concrete – Part I: Definitions, classification specification and conformity – Part II: Test method for measuring first crack strength and ductility indexes. Italian Board for Standardization; 2003.

Valente TDS. Advanced tools for design and analysis of fiber reinforced concrete structures [Doctoral thesis]. Portugal: University of Minho; 2010 (in press).

Vandewalle L. RILEM TC 162-TDF, Test and design methods for steel fibre reinforced concrete r-e design method – Final Recommendation. J Mater Struct 2003; (36):560-7.

Ventura-Gouveia A. Constitutive models for the material nonlinear analysis of concrete structures including time dependent effects [Doctoral thesis]. Portugal: University of Minho; 2011.

Zhang, J., Stang. H.: Application of stress crack width rela- tionship in predicting the flexural behavior of fiber rein- forced concrete. J Cem Concr Research 1998; 28 (3): 439–452.

Figure captions

Fig. 1	(a) Definition of residual strengths, f_{Rj}, and (b) $\sigma - w$ simplified uniaxial constitutive law in accordance with MC2010.
Fig. 2	Nominal flexural stress – CMOD relationship obtained by performing prism bending test.
Fig. 3	Round determinate panel test: (a) setup, (b) dimensions of SRDP, and (c) location of the installed LVDTs.
Fig. 4	Crack patterns of the tested SRDPs.
Fig. 5	Load *vs.* central deflection relationship obtained by testing the SRDPs.
Fig. 6	Schematic stress versus CMOD (*w*) for a FRC.
Fig. 7	Typical load–crack width curve for a SRDP defining values w_j (Minelli and Plizzari 2015).
Fig. 8	Nominal flexural stress – CMOD relationship of the SFRSCC obtained by performing SRDP test, and (b) coefficient of variation calculated for the residual strength of SFRSCC using both SRDP and prism bending tests.
Fig. 9	Comparison of the $\sigma - w$ relationship calculated in accordance with MC2010, Amin *et al.* (2015) and Minelli and Plizzari (2015).
Fig. 10	(a) Typical crack pattern and deformation of the SRDPs, and (b) crack rotation analysis in SRDPs (Salehian *et al.*, 2014).
Fig. 11	(a) Compressive and uncracked tensile stress vs. strain diagrams, and (b) tensile stress vs. crack width relationship of FRC available in DOCROS.
Fig. 12	Flowchart of the method adopted to calculate $F_c^k - \delta_c^k$ relationship for SRDPs.
Fig. 13	Diagrams for modeling the fracture mode I ($\sigma_{n,1}^{cr} = f_{ct}$, $\sigma_{n,2}^{cr} = \alpha_1 \, \sigma_{n,1}^{cr}$, $\sigma_{n,3}^{cr} = \alpha_2 \, \sigma_{n,1}^{cr}$, $\varepsilon_{n,2}^{cr} = \xi_1 \, \varepsilon_{n,u}^{cr}$, $\varepsilon_{n,3}^{cr} = \xi_2 \, \varepsilon_{n,u}^{cr}$) (Ventura-Gouveia 2011).
Fig. 14	(a) Finite element mesh relevant characteristic, load and support conditions of the type of specimen adopted in the inverse analysis, and (b) experimental results vs. numerical prediction of the notched beam bending tests.
Fig. 15	Crack patterns registered in the experimentally tested SRDPs (grey lines) and those considered in the numerical simulations according to the Selehian *et al.* (2014) method.
Fig. 16	Load and deflection relationship obtained analytically using constitutive σ – w law proposed by (a) MC2010, (b) Amin Ali (2017), (c) Minelli and Plizzari (2015) as well as (d) DOCROS, and (e) Femix software, in comparison with the average experimental results.

Table captions

Table-1	FRSCC composition developed in the experimental program.
Table-2	Limit of proportionality and residual flexural strength of the developed FRSCC.
Table-3	Values of the fracture parameters defining the stress-strain softening laws.
Table-4	σ – w values calculated in accordance with the introduced analytical and numerical methods.

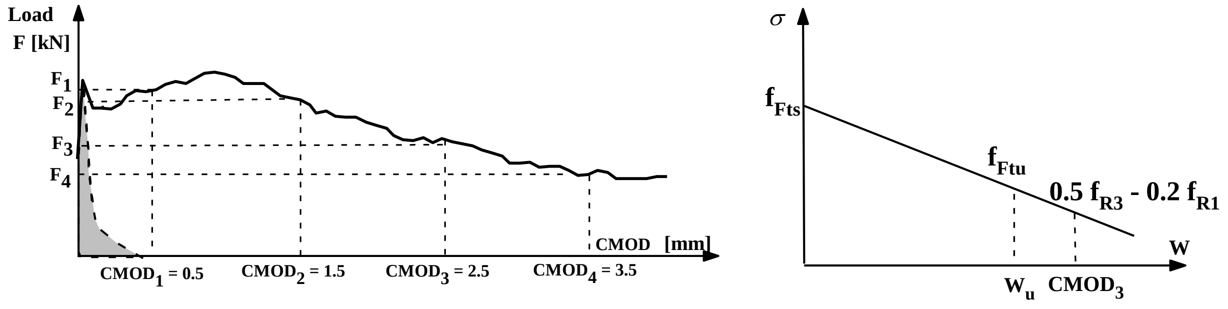

(a) (b)

Fig.1 (a) Definition of residual strengths, f_{Rj} , and (b) $\sigma - w$ simplified uniaxial constitutive law in accordance with MC2010.

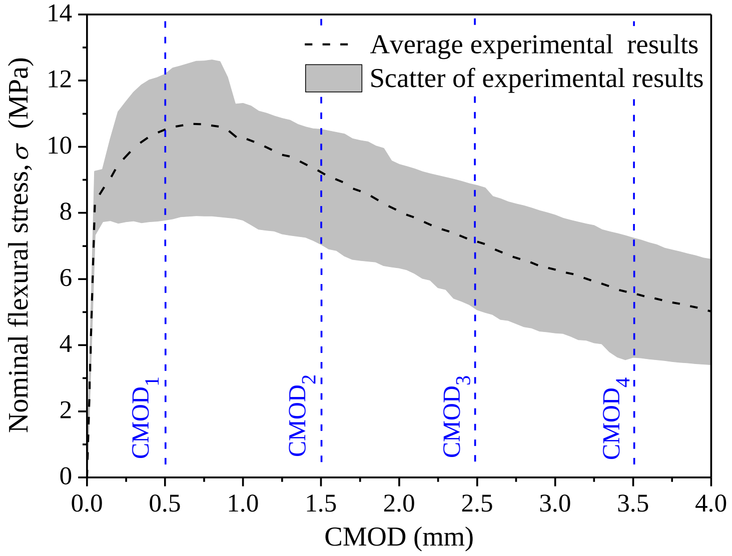

Fig. 2 Nominal flexural stress – CMOD relationship obtained by performing prism bending test.

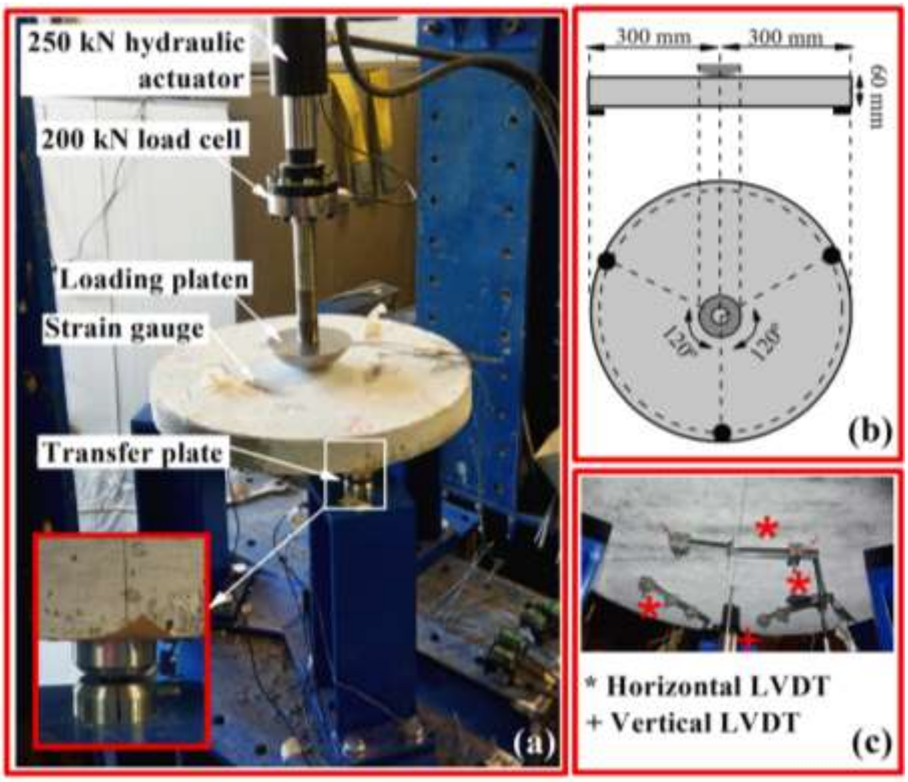

Fig. 3 Round determinate panel test: (a) setup, (b) dimensions of SRDP, and (c) location of the installed LVDTs.

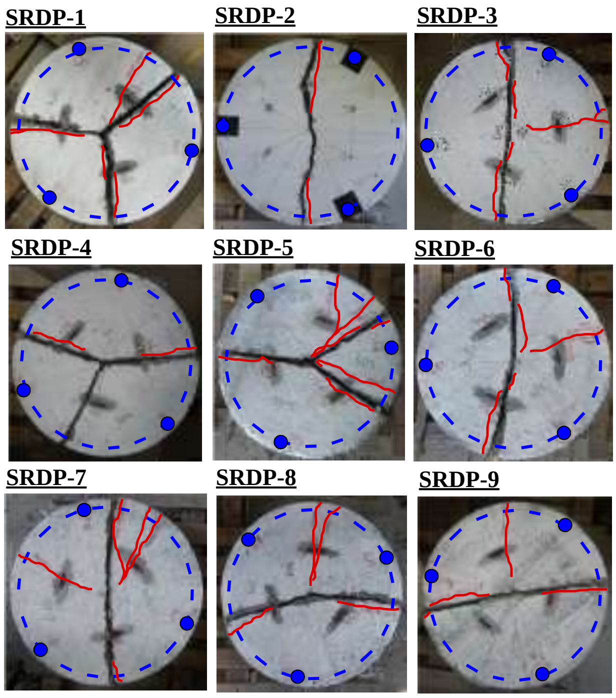

Fig. 4 Crack patterns of the tested SRDPs.

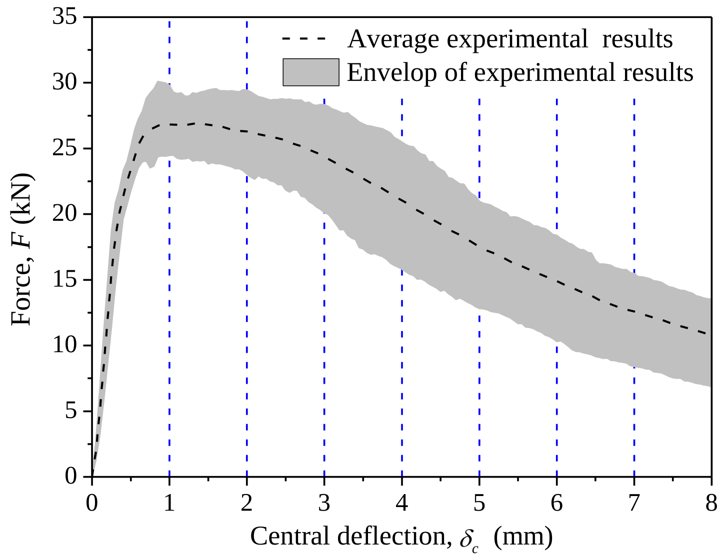

Fig. 5 Load *vs.* central deflection relationship obtained by testing the SRDPs.

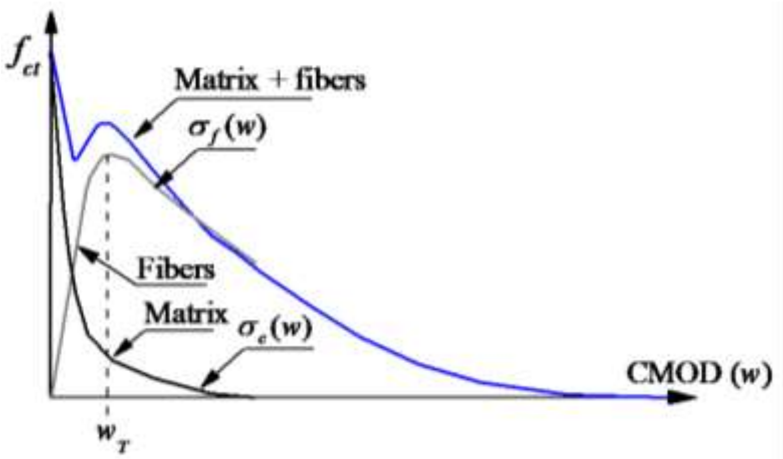

Fig. 6 Schematic stress versus CMOD (w) for a FRC.

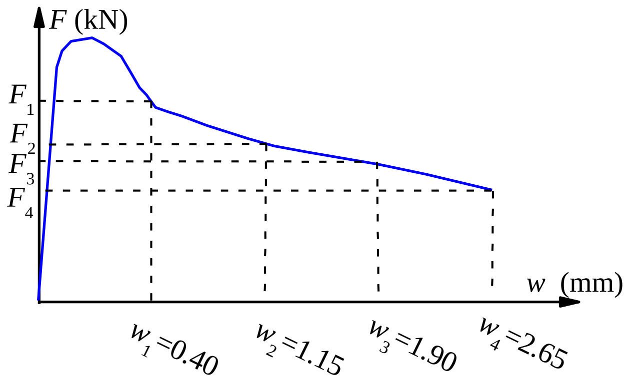

Fig. 7 Typical load–crack width curve for a SRDP defining values w_j (Minelli and Plizzari 2015).

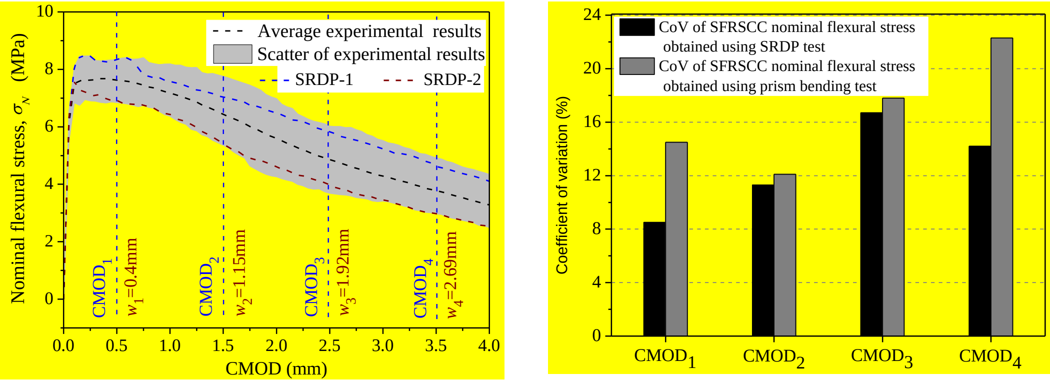

(a) (b)

Fig. 8 (a) Nominal flexural stress – CMOD relationship of the SFRSCC obtained by performing SRDP test, and (b) coefficient of variation calculated for the residual strength of SFRSCC using both SRDP and prism bending tests.

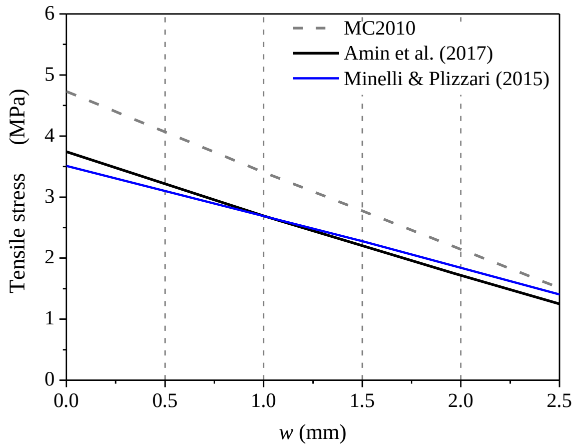

Fig. 9 Comparison of the $\sigma - w$ relationship calculated in accordance with MC2010, Amin *et al.* (2015) and Minelli and Plizzari (2015).

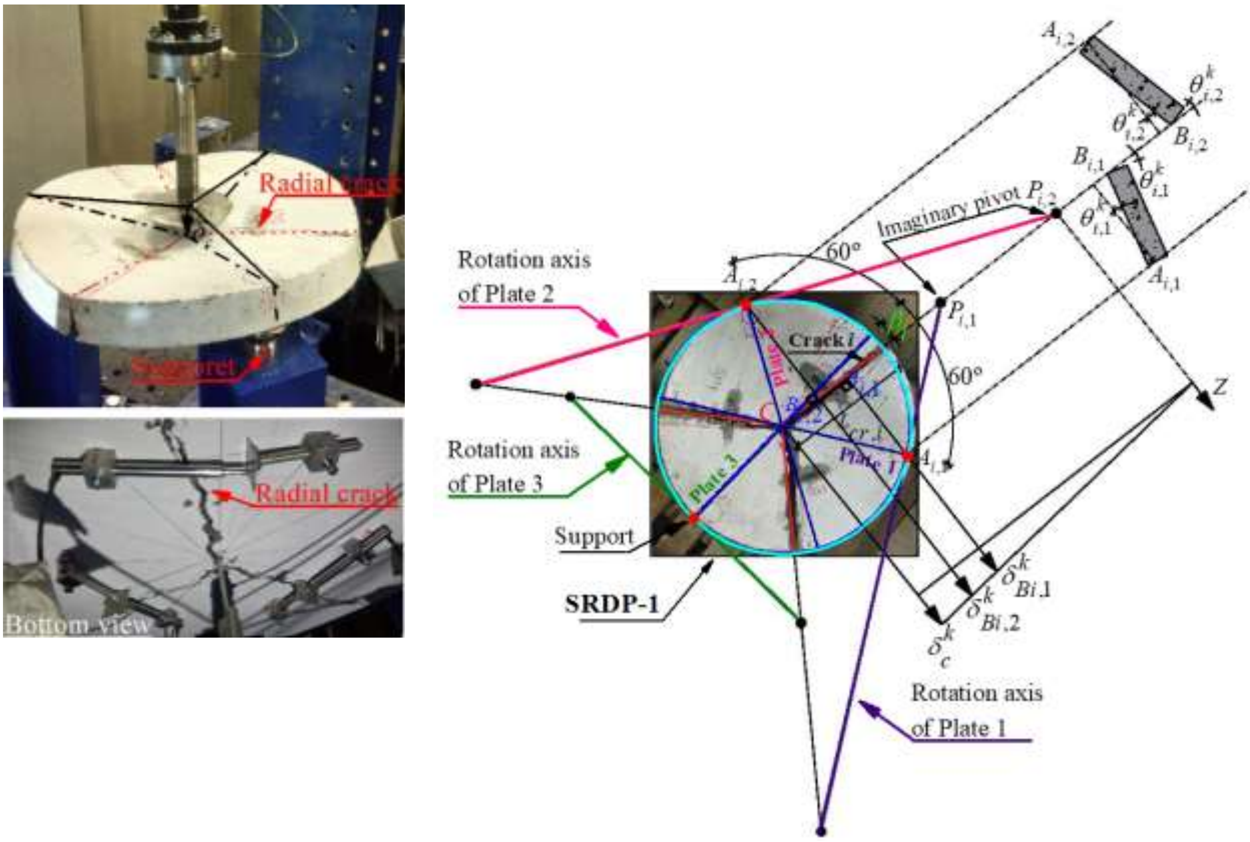

(a) (b)

Fig. 10 (a) Typical crack pattern and deformation of the SRDPs, and (b) crack rotation analysis in SRDPs (Salehian *et al.*, 2014).

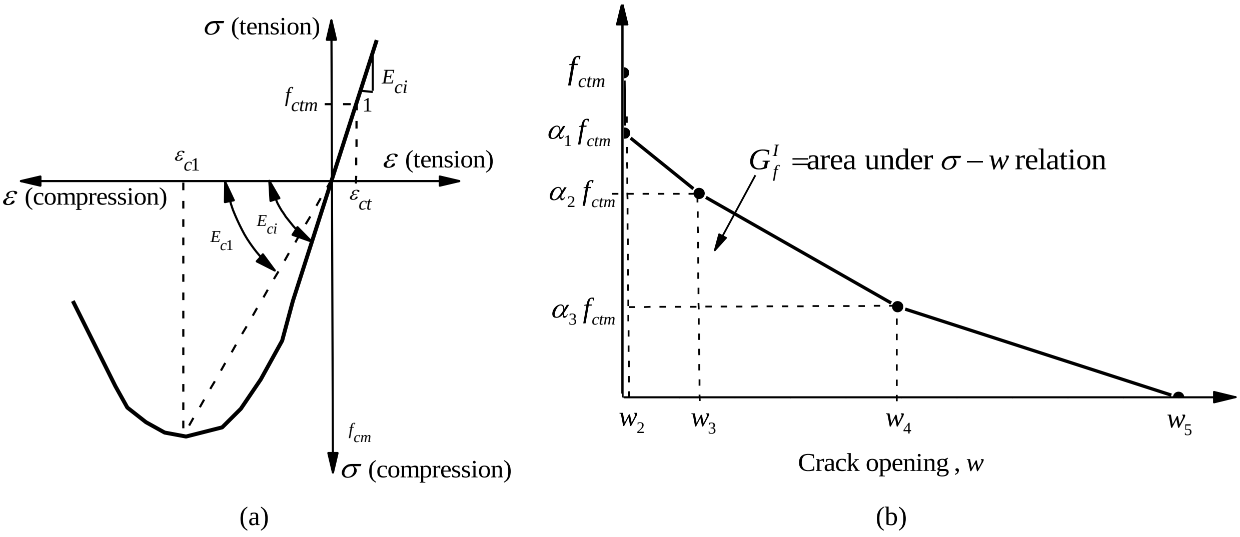

Fig. 11 (a) Compressive and uncracked tensile stress vs. strain diagrams, and (b) tensile stress vs. crack width relationship of FRC available in DOCROS.

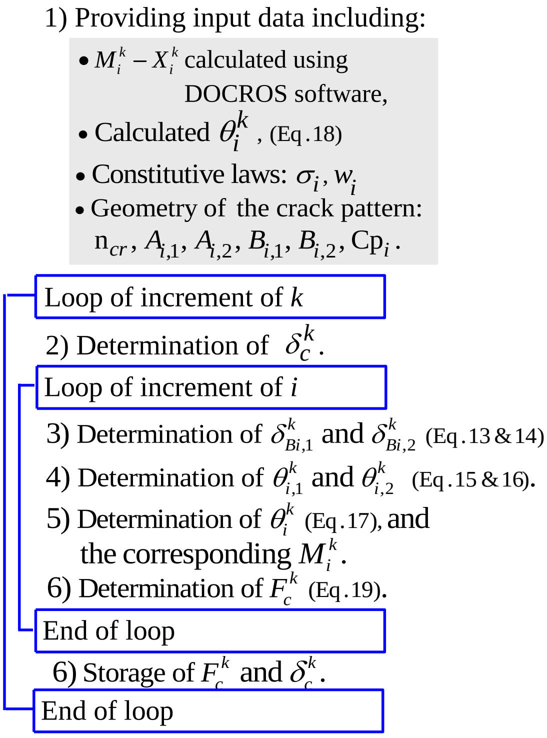

Fig. 12 Flowchart of the method adopted to calculate $F_c^k - \delta_c^k$ relationship for SRDPs.

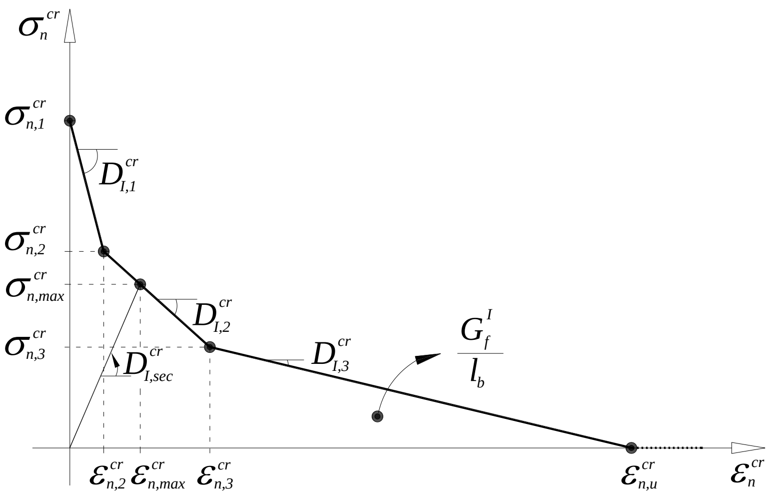

Fig. 13 Diagrams for modeling the fracture mode I ($\sigma_{n,1}^{cr} = f_{ct}$, $\sigma_{n,2}^{cr} = \alpha_1 \sigma_{n,1}^{cr}$, $\sigma_{n,3}^{cr} = \alpha_2 \sigma_{n,1}^{cr}$, $\varepsilon_{n,2}^{cr} = \xi_1 \varepsilon_{n,u}^{cr}$, $\varepsilon_{n,3}^{cr} = \xi_2 \varepsilon_{n,u}^{cr}$) (Ventura-Gouveia 2011).

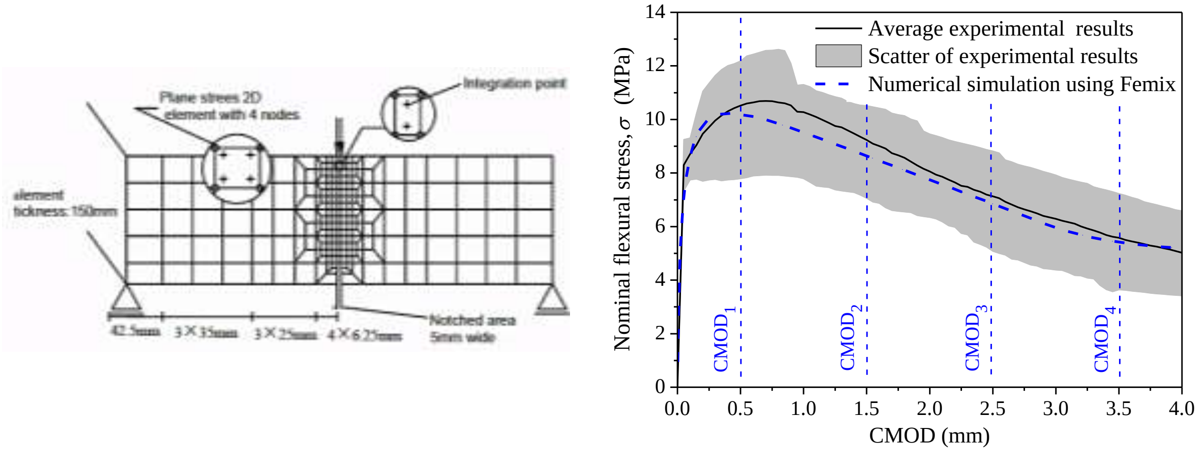

Fig. 14 (a) Finite element mesh relevant characteristic, load and support conditions of the type of specimen adopted in the inverse analysis, and (b) experimental results vs. numerical prediction of the notched beam bending tests.

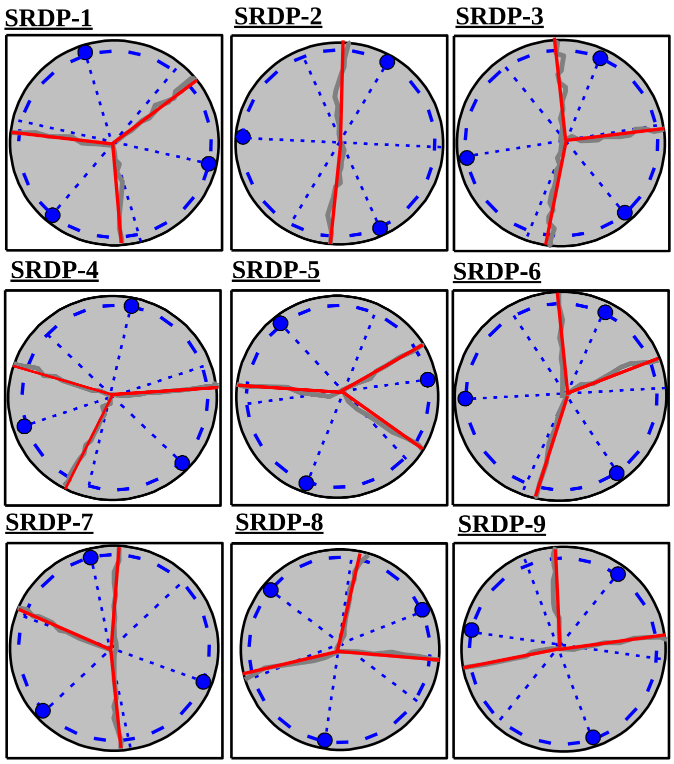

Fig. 15 Crack patterns registered in the experimentally tested SRDPs (grey lines) and those considered in the numerical simulations according to the Selehian *et al.* (2014) method.

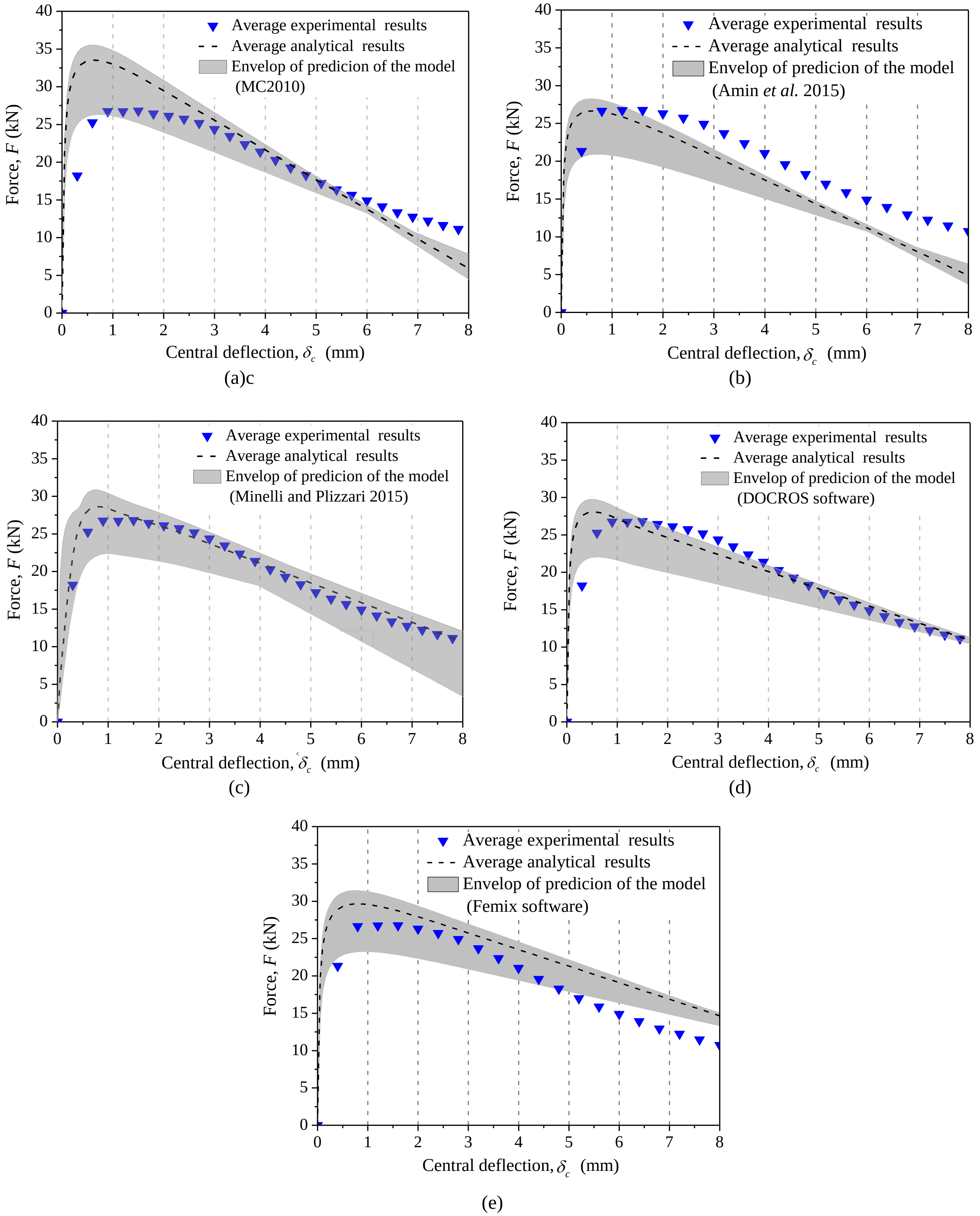

Fig.16 Load and deflection relationship obtained analytically using constitutive σ – w law proposed by (a) MC2010, (b) Amin Ali (2017), (c) Minelli and Plizzari (2015) as well as (d) DOCROS, and (e) Femix software, in comparison with the average experimental results.

Table-1 FRSCC composition developed in the experimental program.

C[a] (kg/m^3)	FA[b] (kg/m^3)	W[c] (L/m^3)	SP[d] (L/m^3)	FS[e] (kg/m^3)	CS[f] (kg/m^3)	CA_{max9mm}[g] (kg/m^3)	$CA_{max12mm}$[h] (kg/m^3)	SF[i] (kg/m^3)	w/b[j] (kg/m^3)
440	131	182	13.14	212	559	205	480	90	0.32

[a] Cement,
[b] Fly ash,
[c] Mixing water,
[d] Superplasticizer,
[e] Fine river sand,
[f] Coarse river sand,
[g] Coarse aggregate of 9 mm maximum diameter,
[h] Coarse aggregate of 12 mm maximum diameter,
[i] Steel fiber,
[j] Water to binder ratio.

Table-2 Limit of proportionality and residual flexural strength of the developed FRSCC.

	$f^{f}_{ct,L}$ (MPa)	f_{R1} (MPa) CMOD$_1$= 0.5	f_{R2} (MPa) CMOD$_2$= 1.5	f_{R3} (MPa) CMOD$_3$= 2.5	f_{R4} (MPa) CMOD$_4$ =3.5	f_{R3k} / f_{R1k} [1]
Average	8.30	10.51	9.24	7.13	5.60	0.63
CoV	7.1%	14.5%	12.1%	17.8%	22.3%	-

[1] f_{R1k} = 8.01 MPa and f_{R3k} = 5.05 MPa.

Table-3 Values of the fracture parameters defining the stress-strain softening laws.

α_1	α_2	α_3	ξ_1	ξ_2	ξ_3	f_{ct} (MPa)	G_f^I (N/mm)
0.93	0.99	0.818	0.0028	0.03	0.2	4	4.3

Table-4 σ – w values calculated in accordance with the introduced analytical and numerical methods.

Crack width (*w*) (mm)	Stress (σ) DOCROS (MPa)	Stress (σ) FEMIX (MPa)	Stress (σ) MC2010 (MPa)	Stress (σ) Amin *et al.* (2015) (MPa)	Stress (σ) Minelli and Plizzari (2015) (MPa)
0.5	3.16	3.67	4.05	3.20	3.05
1	2.80	3.27	3.41	2.69	2.70
2	2.12	2.55	2.15	1.75	1.84
2.5	1.80	2.20	1.52	1.25	1.40